Impact of temperature and gamma radiation on electron diffusion length and mobility in p-type InAs/GaSb superlattices

Jonathan Lee, Chris J. Fredricksen, Elena Flitsiyan, Robert E. Peale, Leonid Chernyak, Zahra Taghipour, Lilian Casias, Alireza Kazemi, Sanjay Krishna, and Stephen Myers

Citation: Journal of Applied Physics **123**, 235104 (2018); doi: 10.1063/1.5030444
View online: https://doi.org/10.1063/1.5030444
View Table of Contents: http://aip.scitation.org/toc/jap/123/23
Published by the American Institute of Physics

Articles you may be interested in

Mid-wavelength high operating temperature barrier infrared detector and focal plane array
Applied Physics Letters **113**, 021101 (2018); 10.1063/1.5033338

Demonstration of long wavelength infrared type-II InAs/InAs$_{1-x}$Sb$_x$ superlattices photodiodes on GaSb substrate grown by metalorganic chemical vapor deposition
Applied Physics Letters **112**, 241103 (2018); 10.1063/1.5035308

Room temperature plasmon-enhanced InAs$_{0.91}$Sb$_{0.09}$-based heterojunction n-i-p mid-wave infrared photodetector
Applied Physics Letters **113**, 011110 (2018); 10.1063/1.5018012

InAs/GaSb type-II superlattice infrared detectors: Future prospect
Applied Physics Reviews **4**, 031304 (2017); 10.1063/1.4999077

Effect of rapid thermal annealing on threading dislocation density in III-V epilayers monolithically grown on silicon
Journal of Applied Physics **123**, 215303 (2018); 10.1063/1.5011161

Tuning the optical properties of InAs QDs by means of digitally-alloyed GaAsSb strain reducing layers
Applied Physics Letters **113**, 103101 (2018); 10.1063/1.5048475

Ultra High Performance SDD Detectors

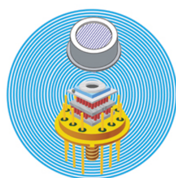

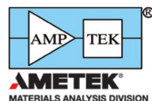

See all our XRF Solutions

JOURNAL OF APPLIED PHYSICS **123**, 235104 (2018)

Impact of temperature and gamma radiation on electron diffusion length and mobility in p-type InAs/GaSb superlattices

Jonathan Lee,[1] Chris J. Fredricksen,[2] Elena Flitsiyan,[1] Robert E. Peale,[1,2] Leonid Chernyak,[1,a)] Zahra Taghipour,[3] Lilian Casias,[3] Alireza Kazemi,[4] Sanjay Krishna,[4] and Stephen Myers[5]

[1]*Department of Physics, University of Central Florida, Orlando, Florida 32816, USA*
[2]*Truventic LLC, 1209 W. Gore St., Orlando, Florida 32805, USA*
[3]*Center for High Technology Materials, University of New Mexico, Albuquerque, New Mexico 87106, USA*
[4]*Department of Electrical and Computer Engineering, The Ohio State University, Columbus, Ohio 43210, USA*
[5]*SK Infrared, 801 University Blvd. SE # 100, Albuquerque, New Mexico 87106, USA*

(Received 21 March 2018; accepted 31 May 2018; published online 18 June 2018)

The minority carrier diffusion length was directly measured by the variable-temperature Electron Beam-Induced Current technique in InAs/GaSb type-II strain-layer-superlattice infrared-detector structures. The Molecular Beam Epitaxy-grown midwave infrared superlattices comprised 10 monolayers of InAs and 10 monolayers of GaSb to give a total absorber thickness of 4 μm. The diffusion length of minority electrons in the p-type absorber region of the *p*-type/barrier/*n*-type structure was found to increase from 1.08 to 2.24 μm with a thermal activation energy of 13.1 meV for temperatures ranging from 77 to 273 K. These lengths significantly exceed the individual 10-monolayer thicknesses of the InAs and GaSb, possibly indicating a low impact of interface scattering on the minority carrier diffusion length. The corresponding minority electron mobility varied from 48 to 65 cm^2/V s. An absorbed gamma irradiation dose of 500 Gy halved the minority carrier diffusion length and increased the thermal activation energy to 18.6 meV, due to creation of radiation-induced defect recombination centers. *Published by AIP Publishing.*
https://doi.org/10.1063/1.5030444

I. INTRODUCTION

The minority carrier diffusion length in semiconductors fundamentally influences the performance of bipolar photodetectors, diodes, and transistors.[1,2] The Electron Beam-Induced Current (EBIC) technique has directly measured the minority carrier diffusion length in several semiconductor materials systems.[2–6] Different collector configurations have been studied, including the normal-collector configuration used here. In contrast to the Schottky configuration (electron beam scanning away from the edge of the Schottky barrier fabricated on the sample surface), the normal-collector configuration (cf. Fig. 1) scans the electron perpendicular to the grown layers.

InAs/GaSb-based type-II strain-layer superlattices (T2SLSs) have recently demonstrated great promise for infrared (IR) detection.[2,7–12] Alternating InAs and GaSb layers of controlled thickness allow tuning of the narrow bandgap from 3 to 30 μm wavelength. The integrated unipolar barrier layer (B) reduces dark current, so that the detectors demonstrate detectivity comparable to conventional HgCdTe detectors.[13] Indeed, a study published by Ramirez *et al*. reports a zero-bias detectivity at 4.5 μm exceeding 10^{10} Jones at 200 K.[10] The primary application for these materials is in IR devices, which may include space, satellite, terrestrial, and military deployment, any of which may be exposed to high energy radiation. Therefore, investigations into radiation effects are necessary to characterize suitability for device deployment in radiation harsh environments.

Residual carrier concentration and transport depend critically on interfacial (InAs/GaSb) roughness, which is controlled by the growth conditions.[14] Further, planar layer deposition leads to anisotropy in the carrier transport properties respective to the growth plane. A critical quantity for detector quantum efficiency is the minority carrier diffusion length, *L*, which is sensitive to defect density and minority carrier scattering. Hence, accurate knowledge of *L* is essential for informed detector optimization.

Previously, EBIC has been used to determine the minority carrier diffusion length in p-type InAs/GaSb T2SLS structures with much different monolayer (ML) ratios. For example, it has been used to estimate the lifetime of excited carriers in a 8/8 ML ratio InAs/GaSb T2SLS by measuring the diffusion length and assuming from Bürkle *et al*. an out-of-plane electron mobility of 1100 cm^2/V s.[2,15] Further, EBIC measurements were taken to observe the impact on the collection efficiency as influenced by the introduction of an InSb interfacial layer in a 9/17 ML ratio InAs/GaSb structure.[16]

This study applies the method of EBIC to determine the impact of gamma irradiation-induced damage on a 10/10 ML ratio InAs/GaSb T2SLS by observing the minority carrier diffusion length and trap thermal activation energy. Gamma irradiation primarily induces ionization defects, but may also produce some displacement defects. Heavy ions, like protons, more readily generate displacement defects, while gamma more easily creates ionization defects. Studies of both types of radiation damage are needed to separate the total ionization dose effects from the displacement effects. In this paper, we report direct measurements of minority carrier

[a)]Electronic mail: leonid.chernyak@ucf.edu

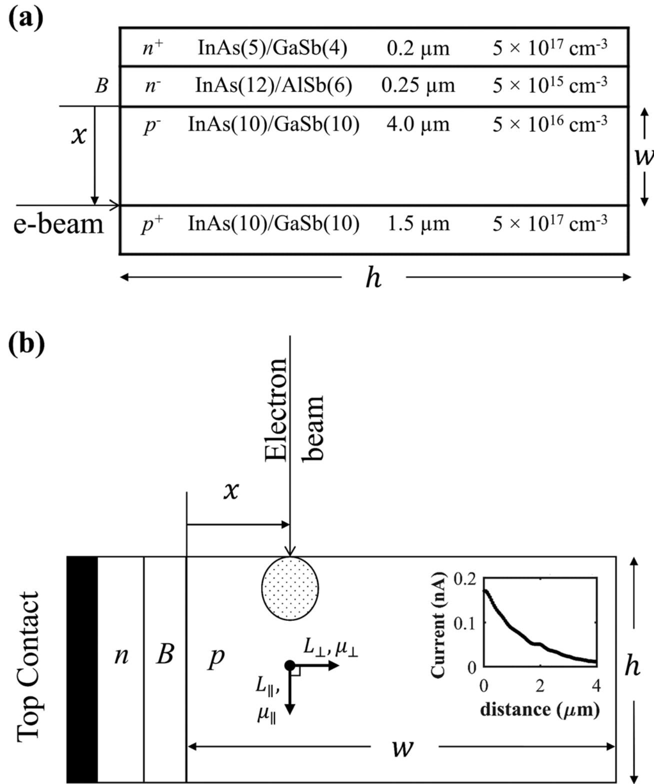

FIG. 1. (a) Schematic of the T2SLS structure. The majority carrier type and concentration, periodic ML ratio, and composite layer thicknesses are indicated. The vertical arrow shows the direction for the EBIC line-scan and the horizontal arrow indicates the instantaneous electron-beam position. The absorber thickness is denoted by w and the sample lateral dimension by h (not to scale). (b) Illustration of the normal-collector configuration. Top metallic contact, n- and p-type regions, absorber thickness w, and sample lateral dimension h (not to scale), and the electron beam-to-junction distance x, are indicated. Carrier transport anisotropy is indicated by $\parallel$ and $\perp$ for L and μ with reference to the growth plane. The **inset** presents typical sample EBIC data. For both diagrams, the barrier (n-type InAs/AlSb) is indicated by the letter "B".

diffusion length, L, perpendicular to the growth plane [also referred to as "out of plane," see Fig. 1(b)] by variable temperature EBIC in InAs/GaSb T2SLS, designed as an IR absorber, to study the ionization dose effects from gamma irradiation.

II. EXPERIMENTAL

The p-type/barrier/n-type (pBn) structure reported here was grown by Molecular Beam Epitaxy (MBE) on a conductive GaSb substrate.[17] This structure is presented schematically in Fig. 1(a), which indicates carrier concentration and type, number and species of monolayers (MLs) in each SL period (e.g., 10/10 for the absorber region), and thicknesses of each region.[18] The bipolar device structure was chosen for analysis due to its potential for practical industrial applications. Specifically, the structure is advantageous due to the higher mobility of minority electrons (relative to holes) in the p-type absorber, which dictates faster bipolar IR detector functionality. The inclusion of a barrier layer has been shown to reduce leakage currents from generation-recombination at interfaces,[9,19] further, due to its lower charge density as compared to the absorber layer, the barrier layer accepts most of the local space charge region.[20] The absorption cutoff wavelength can be estimated to be $\sim$5.8 μm for a 10/10 ML ratio InAs/GaSb T2SLS.[21] Because of its importance for detector quantum efficiency, we focus on the minority carrier diffusion length within the $5 \times 10^{16}\,\text{cm}^{-3}$-doped 4 μm-thick p-InAs/GaSb absorber [cf. Fig. 1(a)]. The absorber layer that is p-type allows for longer potential minority carrier diffusion lengths due to the lower effective mass of excited electrons.

Two identical samples cleaved from the same pBn structure were studied in this work. One was reserved as a control, while the other received a 500 Gy absorbed dose of ^{60}Co gamma irradiation (Nordion, Inc.) at room temperature in a nitrogen environment. (Determination of the absorbed dose value in Gray = Joules/kg includes the substrate.) Gamma radiation was used in order to simulate exposure to a radiation harsh environment. A Ti (5 nm)/Au (50 nm) Ohmic contact was electron-beam evaporated on the top surface of the structure. The back surface of the samples (substrate) was contacted with conductive adhesive. Contacts were applied post irradiation to prevent the possibility of secondary radiation.

The EBIC measurements were carried out *in-situ* on a Philips XL 30 Scanning Electron Microscope (SEM). The contacted sample was mounted on an L-shaped aluminum bracket with grounded bottom contact in the normal-collector configuration, Fig. 1(b). The current from the top contact was amplified and recorded (Stanford Research Systems SR570 current amplifier, Keithley 2000 multimeter, LabView). The SEM beam accelerating voltage was 30 kV, which gives an electron range $R_e \sim 4.8\,\mu$m for both InAs and GaSb employing the Kanaya-Okayama approach.[22,23] The relatively high accelerating voltage optimizes the EBIC resolution, accuracy, and signal-to-noise ratio. Because the EBIC generation region extends laterally by only $\sim\frac{1}{2} R_e$ [cf. Fig. 1(b)], the ratio $R_e/L_e < 4$ ensures the data are not instrument limited.[24] The sample dimension h, which is parallel to the growth plane of the SL (perpendicular to the growth direction, cf. Fig. 1), exceeds 5 mm, which is much larger than the electron range ($h \gg R_e$), so that the dimension, h, does not limit the collection of generated carriers.[4]

The electron beam was scanned along a cleaved edge perpendicular to the growth plane of the layers [cf. Figs. 1(a) and 1(b)] from the top surface to a distance of about 5 μm while recording the induced current. Observing the carrier densities, we may estimate the depletion region width to be approximately 0.4 μm, with $\sim$150 nm extending into the InAs/GaSb absorber p^{-} layer.[20] Carriers diffused from the point of origin at a beam-to-junction distance, x, and some move toward the space-charge region at the n-p InAs/AlSb - InAs/GaSb junction, which separated the non-equilibrium carriers and swept them for collection. Such cross-sectional line-scans were performed at various locations on the cleaved edge for temperatures ranging from 77 to 273 K using a Gatan MonoCL2 temperature-controlled stage monitored by an integrated platinum resistance thermometer with 0.5 K accuracy.

Minority carriers (holes) generated in the n-type region close to the n-p interface [see Figs. 1(a) and 1(b)] do not contribute appreciably to the EBIC signal due to their relatively low mobility ($\mu_p \ll \mu_e$)[25] and the presence of the InAs/AlSb hole-barrier layer blocks hole transport across the junction.[10]

The 1.5 μm thick p^+ region below the absorber [cf. Fig. 1(a)] should also offer minimal interference due to its overall similarity to the 4 μm-thick 10/10 p-InAs/GaSb absorber layer under test.

III. RESULTS AND DISCUSSION

The minority electron diffusion length, L_e, was extracted using methods described in Ref. 6. EBIC, I_E, decays with distance, x, from the junction according to

$$I_E = Ax^{\alpha}\exp\left(-\frac{x}{L_e}\right), \quad (1)$$

where A is a scaling constant. For the normal-collector configuration, this expression is conditionally accurate. The value of the 'linearization coefficient,' α, depends on the surface recombination velocity, v_s. Under the normal-collector configuration, α varies from 0 to $-1/2$ when v_s varies from 0 to ∞, respectively.[6] Equation (1) is the same as used by Hanoka for spherical generation volume and small v_s.[26] The dependence of results on injection density, and comparison of results from Eq. (1) to those from more general models[3,24,27,28] will be presented in a future study. Several EBIC line-scans were completed at each temperature and the average value and standard deviation for minority carrier diffusion length were determined.

The experimental dependence of $\ln(I_E x^{-\alpha})$ on x for the control sample is presented for temperatures 77 and 273 K in Fig. 2 for $\alpha = 0$. The straight line, found when $\alpha = 0$, implies a small value for v_s, below $\sim$1000 cm/s.[6] The diffusion length is determined by the negative reciprocal of the linear slope. The diffusion length for the control sample was found to increase with temperature, as shown in Fig. 3, from the value $1.08 \pm 0.20\,\mu$m at 77 K to $2.24 \pm 0.31\,\mu$m at 273 K. The minority carrier diffusion length far exceeds the InAs and GaSb single-material layer thicknesses of $\sim$2.5 nm, indicating low boundary scattering. This behavior is similar to observations in AlGaN/GaN SLs, where the minority carrier

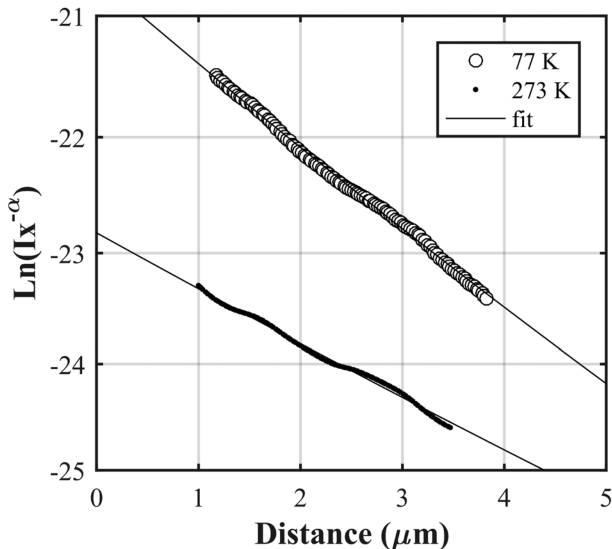

FIG. 2. Control-sample EBIC data and linear fit for temperatures (○) 77 K and (●) 273 K using Eq. (1) employing linearization coefficient, $\alpha = 0$.

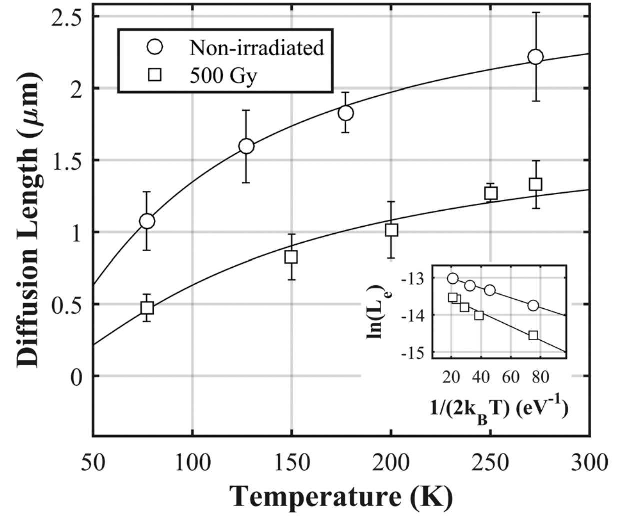

FIG. 3. Temperature dependence of electron diffusion length for the control sample (circles) and 500 Gy gamma-irradiated sample (squares) with exponential fit (solid line) using Eq. (2). **Inset:** Arrhenius plot indicating the corresponding activation energies of 13.1 and 18.6 meV for the non-irradiated and 500 Gy gamma-irradiated samples, respectively.

diffusion length was also found to exceed the SL layer thicknesses.[29] This compares with other reports for InAs/GaSb T2SLS structures, where shortening of diffusion lengths was attributed to interfacial roughness.[2,30] Figure 3 further presents EBIC results for the 500 Gy gamma-irradiated sample, where the L_e values are twice smaller than for the control sample, and E_a has increased to 18.6 meV. The decrease in L_e is reasonably attributed to scattering by radiation-induced defects.

The temperature dependence of the minority electron diffusion length is given by

$$L_e(T) = L_0\exp\left(-\frac{E_a}{2k_B T}\right), \quad (2)$$

where L_0 represents the asymptotic minority carrier diffusion length, k_B is the Boltzmann constant, T is the temperature, and E_a is the activation energy.[1] The value $E_a = 13.1$ meV was found from the temperature dependence presented as an Arrhenius plot in Fig. 3 inset. This value, which is much smaller than the usual bandgaps for mid-wave IR detectors ($\sim$100–400 meV), suggests a thermally activated charge trap or defect level $\sim$13.1 meV below the conduction or above the valence band. The increase in E_a to $\sim$18.6 meV after 500 Gy gamma-irradiation is likely due to the appearance of deeper levels for non-equilibrium carrier recombination, as we previously observed for gamma-irradiated AlGaN/GaN heterostructures.[31]

The minority carrier lifetime, τ, is estimated from the Einstein relation

$$L_e = \sqrt{D\tau}, \quad (3)$$

where diffusivity $D = \mu_e k_B T/q$, μ_e is the minority electron mobility, and q is the electron charge. The lifetime of similar SLS InAs/GaSb structures with an ML ratio of 8/8 was determined by time resolved photoluminescence (TRPL) and was

found to depend on the carrier concentration, therefore at a concentration of $5 \times 10^{16}\,\text{cm}^{-3}$ we assume a temperature independent lifetime of $\tau \sim 36\,\text{ns}$.[32] The minority electron mobility can thus be estimated by

$$\mu_e = \frac{L_e^2 q}{k_B T \tau} \tag{4}$$

and is displayed in Fig. 4 along with line of fit applied using Eq. (4). The electron mobility for *n*-type T2SLS with a ML ratio of 9/9, measured in the SL growth plane ($\mu_{\parallel}$) by quantitative mobility spectrum analysis, was found to b $\sim 1 \times 10^4$ cm^2/V s at 300 K.[25] However, the anisotropy of minority carrier transport leads to a reduction in electron mobility perpendicular to the growth plane—by as much as a factor of 10, according to Bürkle *et al.*, where the electron mobility perpendicular to the growth plane ($\mu_{\perp}$) of a superlattice structure with InAs/(GaIn)Sb of ML ratio 8/8 was measured to be $\sim$1100 cm^2/V s, though the overall structure is intrinsically different than this case.[2,15] Here, the mobility perpendicular to the growth plane for minority electrons in the non-irradiated *p*-type T2SLS with ML ratio 10/10 was found to be $\sim$55 cm^2/V s at 300 K. The comparatively low value of electron mobility is attributed to possible differences in the layer content, carrier concentration, ML ratio, and interfacial roughness.

For the non-irradiated sample, there is an apparent shift in the trend of the minority electron mobility near 120 K shown in Fig. 4 which is characteristic of this T2SLS structure,[7,11,18,25] where a shift in the majority carrier mobility and density was observed for InAs/GaSb SLs with 8/8 and 9/9 periodic ML ratios. In those cases, the inflection was attributed to a shift in the dominant scattering mechanism from impurity scattering at low temperatures to phonon scattering at high temperatures. For the 500 Gy gamma-irradiated sample, the behavior of the mobility suggests a transition of the dominant scattering mechanism may occur at $\sim$200 K, and is likely due to scattering on radiation induced defects.

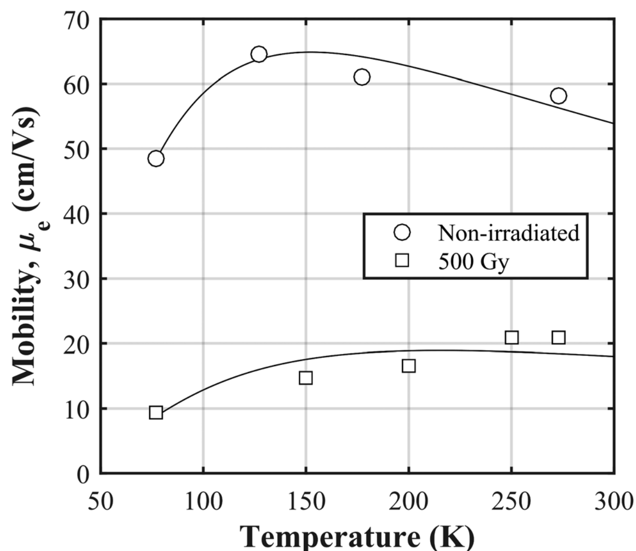

FIG. 4. Electron mobility values for the control sample (circles) and 500 Gy gamma irradiated sample (squares) and the corresponding fit (solid lines) using Eqs. (2) and (4) and assuming $\tau = 36\,\text{ns}$ after Ref. 32.

IV. CONCLUSIONS

In summary, the minority carrier diffusion length in non-irradiated InAs/GaSb T2SLS was directly measured by EBIC and found to follow a simple Boltzmann temperature dependence with an activation energy of 13.1 meV. The linearization coefficient, α, was estimated to be 0, implying negligible surface recombination velocity. Gamma irradiation with a modest 500 Gy dose decreased the electron diffusion length by twice and correspondingly increased the thermal activation energy to 18.6 meV. Electron mobilities were estimated based on the experimentally obtained L_e values perpendicular to the growth plane and independent lifetime studies. The room temperature control sample minority electron mobility was found to be $\sim$55 cm^2/V s and reduced to $\sim$21 cm^2/V s after 500 Gy gamma irradiation. The increase in activation energy and decrease in mobility is attributed to radiation-induced scattering centers and deep levels for non-equilibrium carrier recombination.

ACKNOWLEDGMENTS

Research at UCF was supported in part by the National Science Foundation Award No. ECCS 1624734 and the US-Israel BSF Award Nos. 2014020, AFRL FA 9453-14-1-0248, and ARO W911NF-16-2-0068. Contributions by C.J.F. were funded by an MDA Phase I SBIR to Truventic, Contract No. HQ014717C7256P00001. C.J.F. and R.E.P. are members of Truventic LLC and may benefit financially from the results of the research presented here.

[1]L. Chernyak, A. Osinsky, and A. Schulte, Solid-State Electron. **45**(9), 1687 (2001).
[2]J. V. Li, S. L. Chang, E. M. Jackson, and E. Aifer, Appl. Phys. Lett. **85**(11), 1984 (2004).
[3]F. Berz and H. K. Kuiken, Solid-State Electron. **19**(6), 437 (1976).
[4]O. Kurniawan and V. K. S. Ong, in *Proceedings of the Optoelectronic and Microelectronic Materials and Devices* (IEEE, Perth, WA, Australia, 2006).
[5]V. K. S. Ong, J. C. H. Phang, and D. S. H. Chan, Solid-State Electron. **37**(1), 1 (1994).
[6]C. C. Tan, V. K. S. Ong, and K. Radhakrishnan, IEEE Trans. Electron Devices **60**(10), 3541 (2013).
[7]C. Cervera, J. B. Rodriguez, J. P. Perez, H. Ait-Kaci, R. Chaghi, L. Konczewicz, S. Contreras, and P. Christol, J. Appl. Phys. **106**, 033709 (2009).
[8]V. M. Cowan, C. P. Morath, S. Myers, E. Plis, and S. Krishna, Proc. SPIE **8353**, 83530F (2012).
[9]E. A. Plis, Adv. Electron. **2014**, 246769.
[10]D. A. Ramirez, E. A. Plis, S. Myers, L. A. Treider, E. Garduno, C. P. Morath, V. M. Cowan, and S. Krishna, Proc. SPIE **9226**, 92260Q (2014).
[11]A. Haddadi, R. Chevallier, A. Dehzangi, and M. Razeghi, Appl. Phys. Lett. **110**, 101104 (2017).
[12]L. A. Treider, C. P. Morath, V. M. Cowan, Z. B. Tian, and S. Krishna, Infrared Phys. Technol. **70**, 70 (2015).
[13]A. Rogalski and P. Martyniuk, Infrared Phys. Technol. **48**, 39 (2006).
[14]T. V. C. Rao, S. V. Nair, H. E. Ruda, J. Antoszewski, J. B. Rodriguez, E. Plis, S. Krishna, and L. Faraone, Semicond. Sci. Technol. **27**, 105025 (2012).
[15]L. Bürkle, F. Fuchs, R. Kiefer, W. Pletschen, R. Sah, and J. Schmitz, Mater. Res. Soc. Symp. Proc. **607**(75), 77 (1999).
[16]D. Zuo, P. Qiao, D. Wasserman, and S. L. Chuang, Appl. Phys. Lett. **102**, 141107 (2013).
[17]E. Plis, S. Annamalai, K. T. Posani, S. Krishna, R. A. Rupani, and S. Ghosh, J. Appl. Phys. **100**, 014510 (2006).
[18]T. V. C. Rao, J. Antoszewski, L. Faraone, J. B. Rodriguez, E. Plis, and S. Krishna, Appl. Phys. Lett. **92**, 012121 (2008).
[19]J. R. Pedrazzani, S. Maimon, and G. W. Wicks, Electron. Lett. **44**(25), 1487 (2008).

[20]S. M. Sze, *Semiconductor Device Physics and Technology* (Wiley, New York, 1985).
[21]P. Christol and J. B. Rodriguez, Proc. SPIE **10563**, 105632C (2014).
[22]K. Kanaya and S. Okayama, J. Phys. D: Appl. Phys. **5**, 43 (1972).
[23]O. Kurniawan and V. K. S. Ong, Scanning **29**(6), 280 (2007).
[24]K. L. Luke, O. von Roos, and L.-J. Cheng, J. Appl. Phys. **57**(6), 1978 (1985).
[25]T. V. C. Rao, J. Antoszewski, J. B. Rodriguez, E. Plis, S. Krishna, and L. Faraone, J. Vac. Sci. Technol. B **26**(3), 1081 (2008).
[26]J. I. Hanoka and R. O. Bell, Annu. Rev. Mater. Sci. **11**, 353 (1981).
[27]S. I. Maximenko, L. Mazeina, Y. N. Picard, J. A. Freitas, Jr., V. M. Bermudez, and S. M. Prokes, Nano Lett. **9**(9), 3245 (2009).
[28]J.-M. Bonard and J.-D. Ganiere, J. Appl. Phys. **79**(9), 6987 (1996).
[29]L. Chernyak, A. Osinsky, V. N. Fuflyigin, J. W. Graff, and E. F. Schubert, IEEE Trans. Electron Devices **48**(3), 433 (2001).
[30]C. A. Hoffman, J. R. Meyer, E. R. Youngdale, F. J. Bartoli, R. H. Miles, and L. R. Ram-Mohan, Solid-State Electron. **37**(4–6), 1203 (1994).
[31]C. Schwarz, A. Yadav, M. Shatkhin, E. Flitsiyan, L. Chernyak, V. Kasiyan, L. Liu, Y. Y. Xi, F. Ren, S. J. Pearton, C. F. Lo, J. W. Johnson, and E. Danilova, Appl. Phys. Lett. **102**, 062102 (2013).
[32]B. Klein, N. Gautam, E. Plis, T. Schuler-Sandy, T. J. Rotter, and S. Krishna, J. Vac. Sci. Technol. B **32**, 02C101 (2014).